Hindawi Publishing Corporation
International Journal of Photoenergy
Volume 2014, Article ID 928519, 7 pages
http://dx.doi.org/10.1155/2014/928519

Research Article

Photocatalytic Degradation of Rhodamine B Dye over Novel Porous TiO_2-SnO_2 Nanocomposites Prepared by Hydrothermal Method

Yan Wang,[1] Zhaoli Yan,[2] and Xiaodong Wang[2]

[1] *School of Safety Science and Engineering, Henan Polytechnic University, Jiaozuo, Henan 454000, China*
[2] *School of Materials Science and Engineering, Henan Polytechnic University, Jiaozuo, Henan 454000, China*

Correspondence should be addressed to Xiaodong Wang; wangxd0863@aliyun.com

Received 23 January 2014; Accepted 16 February 2014; Published 19 March 2014

Academic Editor: Tian-Yi Ma

The photocatalytic degradation of Rhodamine B dye was successfully carried out under UV irradiation over porous TiO_2-SnO_2 nanocomposites with various molar ratios of Ti/Sn (4–12) synthesized by hydrothermal method using polystyrene microspheres as template. The combination of TiO_2 with SnO_2 can obtain high quantum yield of TiO_2, and then achieve the high photocatalytic activity. And its porous structure can provide large surface area, leading to more adsorption and fast transfer of dye pollutant. Structural and textural features of the samples were investigated by X-ray diffraction (XRD), transmission electron microscopy (TEM), and N_2 sorption techniques. Both adsorption and UV irradiation contribute to decolorization of about 100% of Rhodamine B dye over the sample TiSn10 after 30 min of the photocatalytic reaction, while the decomposition of Rhodamine B dye is only 62% over pure titania (Degussa P25).

1. Introduction

The disposal of various toxic dyes from the textile industry has attracted extensive attention in the field of water pollution prevention and cure. Rhodamine B (RB) is one of the famous dyes and is widely used as a colorant in foodstuffs and textiles due to its high stability. It is harmful to human beings and animals and causes irritation of the skin, eyes, and respiratory tract. The removal methods of toxic dyes have been considered in recent studies in the literature. These include physical adsorption [1, 2], chemical degradation [3], biological degradation [4], photodegradation, or the synergic treatments of different methods. Recently, much attention has been paid to the photocatalytic degradation of dye pollutants using nanodispersed catalysts TiO_2 [5], SnO_2 [6], and so forth. It uses light energy to initiate chemical reactions in the presence of photocatalysts which are mostly semiconductor materials. Heterogeneous photocatalysis using semiconductors is an effective and rapid technique for the removal of dye pollutants from wastewater [7].

TiO_2 is regarded as a promising semiconductor in degradation of various dye pollutants for its strong oxidizing power, nontoxicity, low cost, chemical stability, and high photocatalytic activity [8]. The degradation process involves the exposure of TiO_2 to UV light which is associated with formation of positive hole and negative electrons in the valence and conduction bands that oxidize and reduce the dye pollutants. However, there are some issues that limit the photocatalytic activity of TiO_2 materials, such as the low quantum yield, the wide band gap energy (3–3.2 eV), and the low mass transport **a**rates. Therefore, the researchers conduct many works to solve these essential drawbacks. An effective strategy is to couple TiO_2 with other semiconductors, transition elements, and noble metals which can improve the photodegradation activity owing to the role of dopants in improving the optical features of the samples by extending the absorption activity to visible region and preventing the recombination of the charge carriers [9–12]. And another useful means is to increase its surface area via synthesis of porous TiO_2 monoliths, leading to more adsorption and fast transfer of dye pollutants. More attention has been paid to $Sn_xTi_{1-x}O_2$ system in recent years by coupling TiO_2 with SnO_2 [13–17]. It is generally accepted that this new nanocomposite exhibits high photocatalytic reactivity compared with pure TiO_2. It is well known that the

band gaps of SnO_2 and TiO_2 are 3.6 and 3.2 eV, respectively. The combination of these two semiconductors leads to the accumulation of electron in the conduction band of SnO_2 and the photogenerated holes in the valence band of the TiO_2 particle, which improve the separation of photogenerated charges, shifting the photoexcitation of the sample toward visible light, and increase the oxidizing power of TiO_2 [14–16].

In this work, we reported a novel hierarchical macroporous-mesoporous TiO_2-SnO_2 nanocomposite prepared by hydrothermal method using polystyrene microspheres as template. The textural and structural properties of the as-prepared photocatalysts were characterized by means of XRD, TEM, and N_2 sorption. And the photocatalytic activities of the as-prepared catalysts were evaluated by the photocatalytic degradation of RB dye pollutant under UV light. The effect of the molar ratios of Ti/Sn on the crystal structure, morphology, and optical properties of the final products was investigated.

2. Experimental Section

2.1. Materials. Titanium n-butoxide (TBOT, $Ti(OC_4H_9)_4$), tin(IV) chloride, tetrahydrofuran (THF), and acetone were used without any further purification. All chemicals used in this study were of analytical grade and purchased from Sinopharm Chemical Reagent Co., Ltd. or Tianjin Dengke Chemical Reagent Co., Ltd. Polystyrene (PS) microspheres were obtained by emulsion polymerization of styrene which had been discussed in our previous reports [18, 19]. In a typical procedure, 150 g deionized water was poured into a 300 mL jacket reactor, which was kept at 85°C until the end of the reaction. Then, 0.075 g sodium styrene sulfonate and 0.0633 g sodium hydrogen carbonate were dissolved in the deionized water. Under constant stirring, 17.50 mL styrene monomer was added to this solution under the nitrogen protection. After 1 h, 0.0833 g potassium persulfate was introduced into the solution. After 18 h polymerization, the monodispersed PS spheres with the diameter of 247 nm were obtained.

2.2. Preparation of TiO_2-SnO_2 Composites. The TiO_2-SnO_2 photocatalysts were prepared by hydrothermal method using polystyrene microspheres as template. In a typical procedure, 1.052 g $SnCl_4{\cdot}5H_2O$ and the calculated volume of TBOT with various molar ratios of Ti/Sn (4–12) were dissolved in 60 mL of anhydrous ethanol under stirring; then the calculated amount of PS microspheres (100 g PS microspheres per mole of solutes) was added to the prepared solution under magnetic stirring. After ultrasonic dispersion for 20 min, the distilled water was slowly dripped into the resulting suspension under vigorous stirring until the gel occurred; then distilled water for diluting the suspension continued to be added (ensure that the total volume of distilled water is 200 mL) and stirred for 30 min. Subsequently, the pH value of the suspension was regulated by adding aqueous ammonia and simultaneous stirring until pH = 8 and kept for 30 min. The solution and the resulting precipitates were placed inside a Teflon-lined stainless autoclave, and the autoclave was heated at 150°C for 5 h. Then the mixture was cooled down to room temperature and the precipitate was separated by filtration, washed several times with distilled water and anhydrous ethanol, and dried 10 h in air at 60°C. Finally, the obtained sample was placed in a glass soxhlet extractor and PS microspheres were extracted by the mixed solution of THF/acetone (1/1 of v/v) for four days, dried 6 h in air at 80°C, and ground to 60–80 mesh. The series of as-prepared samples were named as TiSn4, TiSn6, TiSn8, TiSn10, and TiSn12 corresponding to the samples with various molar ratios of Ti/Sn = 4, 6, 8, 10, and 12, respectively.

2.3. Characterization. X-ray diffraction (XRD) analysis was performed on a Bruker-AXS D8 Advance diffractometer, with CuK_α radiation at 40 kV and 25 mA in a scanning range of 10–80° (2θ). The diffraction peaks of the crystalline phase were compared with those of standard compounds reported in the JCPDS Data File. N_2 adsorption-desorption isotherms were collected at liquid nitrogen temperature using a Micromeritics ASAP 2020 adsorption apparatus. Before carrying out the measurement, each sample was degassed at 60°C for more than 6 h. The specific surface areas (S_{BET}) of the samples were calculated following the multipoint BET (Brunauer-Emmett-Teller) procedure. The pore size distributions were determined from the adsorption branch of the isotherms using the BJH method. Transmission electron microscopy (TEM) analysis was performed on a JEOL JEM-2100 microscope, operating at 200 kV. The samples were dispersed in ethanol and treated with ultrasound for 5 min and then deposited on a copper grid coated with preformed holey carbon film.

2.4. Photocatalytic Activity Measurements. Rhodamine B aqueous solution under UV light was used as a model reaction to evaluate the photocatalytic activity of prepared samples. The light source was a 450 W high-pressure mercury lamp (center wavelength = 365 nm, Foshan Electrical And Lighting Co., Ltd., China) and the lamp was located 15 cm higher than the solution surrounded by a circulating water tube. A general procedure was carried out as follows. First, 100 mL aqueous Rhodamine B solution (20 mg/L) was placed in a 500 mL water-jacketed reactor, which was maintained at a temperature of 20°C. Then, 0.1 g catalyst was suspended in the solution. The suspension was stirred in dark for 30 min in order to reach the adsorption-desorption equilibrium. Finally, the suspension was irradiated under UV light. To monitor the photocatalytic process, 6 mL mixture solution was aspirated from the test tube with an interval of 10 min. The determination of Rhodamine B (RB) dye was done on a TU-1810 UV-vis spectrophotometer by measuring absorbance at λ_{max} of 553 nm. A calibration curve obtained at the RB dye concentration of 1–10 mg/L was used for determination of initial and final concentrations. The photocatalytic degradation rate was calculated by the following expression:

$$\text{Degradation rate } (\%) = \frac{C_0 - C}{C_0} \times 100\%, \quad (1)$$

where C_0 (mg/L) is the initial concentration of Rhodamine B solution which reached absorbency balance and C (mg/L) is

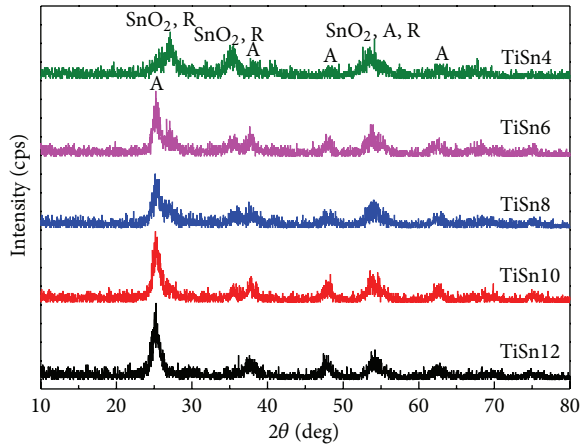

FIGURE 1: XRD patterns of the prepared samples TiSn4, TiSn6, TiSn8, TiSn10, and TiSn12.

the concentration of the dye solution at the irradiation time (t).

3. Results and Discussion

3.1. Characterization of Nanoparticles

3.1.1. X-Ray Diffraction. Figure 1 shows the typical XRD patterns of the as-prepared samples TiSn4, TiSn6, TiSn8, TiSn10, and TiSn12. When the molar ratios of Ti/Sn > 4, the diffraction peaks at $2\theta = 25.2$, 37.8, 48, 53.9, and 62.6° reveal the existence of predominant anatase phase (JCPDS number 21-1272). And, the relatively weak peaks detected at $2\theta = 27.2$, 35.5, and 53.5° are referred to as rutile phase (JCPDS number 21-1276). Simultaneously, along with the molar ratios of Ti/Sn decrease (which means the increase of SnO_2 content), the peaks intensity of anatase phase decreased and that of rutile phase was enhanced. When the molar ratios of Ti/Sn = 4, the main phase of TiO_2 converts to rutile phase. The diffraction peaks showed at $2\theta = 26.6$, 34.8, and 52.8° are referred to as cassiterite phase (JCPDS number 41-1445), and they are enhanced with the decrease of the molar ratios of Ti/Sn. On examining the figure, one can notice that the SnO_2 content impacts the crystalline phase of TiO_2 significantly. The excessive SnO_2 can make the main phase of TiO_2 convert from anatase to rutile phase. In addition, the sharp peaks in Figure 1 indicate the well crystallization of all the samples via the hydrothermal action.

3.1.2. TEM Analysis of TiO_2-SnO_2 Nanoparticles. Figure 2 shows the low resolution TEM (LRTEM) images of the prepared TiSn10 nanoparticles from different areas. The images clearly demonstrate that the TiSn10 sample has a disordered spherical macroporous structure, formed by the agglomeration of the uniform nanoparticles on the surface of polystyrene microspheres and the extraction of polystyrene microspheres by the mixed solution of THF/acetone. The average pore size of spherical macropores is about 580 nm, and it is obviously larger than the average particle size 247 nm of polystyrene microspheres. This may be owing to the fact that the temperature of hydrothermal reaction (150°C) is higher than the glass transition temperature of polystyrene microspheres (120°C), which leads to the flow and fusion of liquefied polystyrene microspheres. Furthermore, it also can be seen that the spherical macroporous structure has been slightly damaged due to the hydrothermal action and grind during the preparation process.

The TEM images of the walls of spherical macropores recorded at different magnification are displayed in Figure 3. It clearly demonstrates that the walls of spherical macropore have a disordered mesoporous structure, which is formed by the agglomeration of the uniform nanoparticles. The accessible mesopores are connected randomly, lacking discernible long-range order in the pore arrangement among the small particles. And the nanoparticles in the sample are of regular morphology with the size around 10 nm (Figure 3(b)). In conclusion, the as-prepared TiSn10 sample has a hierarchical macroporous-mesoporous structure formed by nanoparticles.

3.1.3. N_2-Sorption Analysis. Figure 4 depicts N_2 adsorption-desorption isotherms and the corresponding pore size distribution curves of the prepared samples TiSn4, TiSn6, TiSn8, TiSn10, and TiSn12. The textural properties of the samples are listed in Table 1. The surface area of TiSn4 and TiSn10 is 71 m^2/g and 73 m^2/g, respectively, while the total pore volume of them is 0.28 cm^3/g and 0.23 cm^3/g, respectively. The highest surface area and pore volume (162 m^2/g and 0.51 cm^3/g) are obtained by the TiSn8 sample. From Figure 4(a), it can be seen that the isotherms of all the prepared samples are of classical type IV, characteristic of mesoporous materials according to the IUPAC, and the adsorption isotherms of the samples TiSn4, TiSn6, TiSn8, and TiSn10 exhibit a large increase at the P/P_0 above 0.8, indicating the presence of the macroporous structure (consistent with the TEM analysis results in Figures 2 and 3). In comparison to the well-known nonporous TiO_2 material (P25), the hierarchical macroporous-mesoporous structure of the prepared samples is believed to facilitate the absorption of RB dye (Table 2) and the transport of photodegradation product molecules. The pore size distribution curves of the prepared samples, which are determined by the BJH method from the adsorption branch of the isotherm, exhibit one single narrow peak centered at 7.7–13.9 nm (Figure 4(b)), indicating the good homogeneity of the pores. Besides, one can observe a progressive increase in average pore size upon decreasing the molar ratios of Ti/Sn from 12 to 4 (namely, increasing the SnO_2 content from 7.7 to 20.0%).

3.2. Photocatalytic Activity Studies. Figure 5 displays the photocatalytic degradation rate and the pseudo-first-order kinetics of the prepared samples and pure TiO_2 (P25, the surface area of 50 m^2/g). The absorption (in dark) and photodegradation rates (under UV light) of RB dye by different photocatalysts within 30 min are presented in Table 2. From Figure 5(a), it is seen that all the prepared TiO_2-SnO_2 composites possess high degradation rate compared with pure titanium oxide P25, indicating the effectiveness of SnO_2

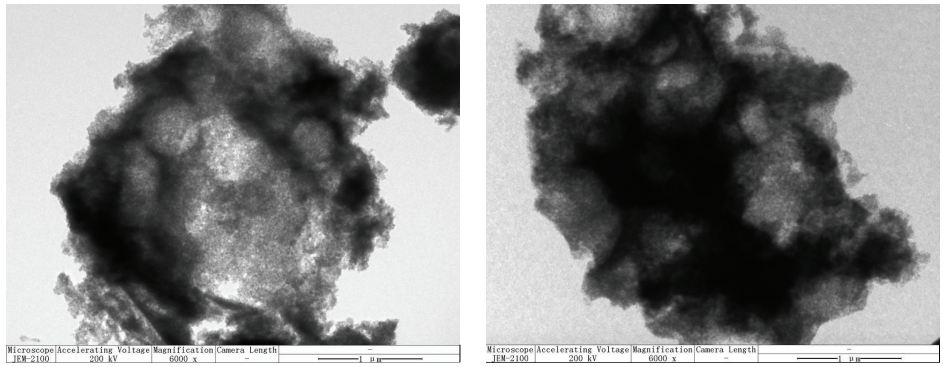

(a) (b)

Figure 2: LRTEM (Low resolution TEM) images of the prepared TiSn10 nanoparticles.

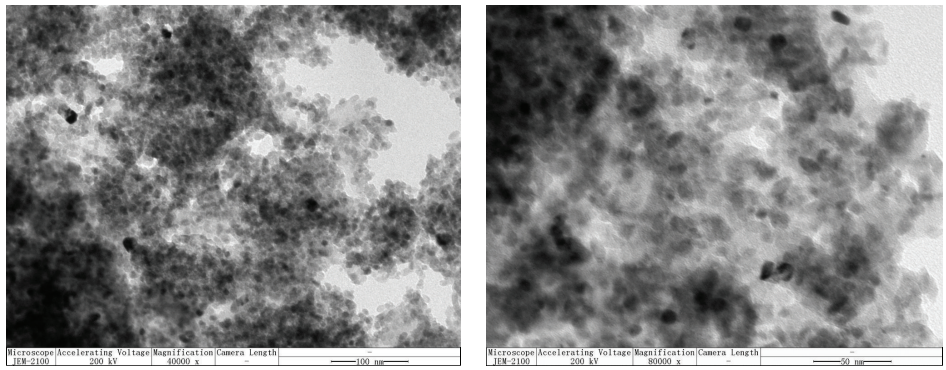

(a) (b)

Figure 3: TEM images of the prepared TiSn10 nanoparticles.

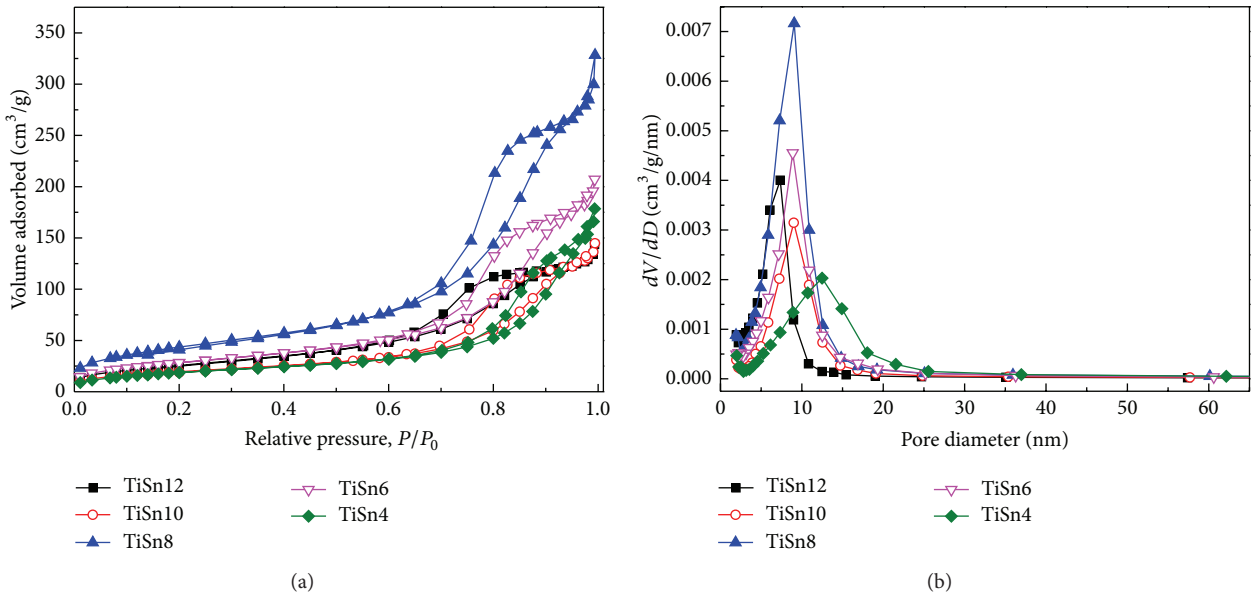

Figure 4: (a) N_2 adsorption-desorption isotherms and (b) the corresponding pore size distribution curves of the prepared samples: TiSn4, TiSn6, TiSn8, TiSn10, and TiSn12.

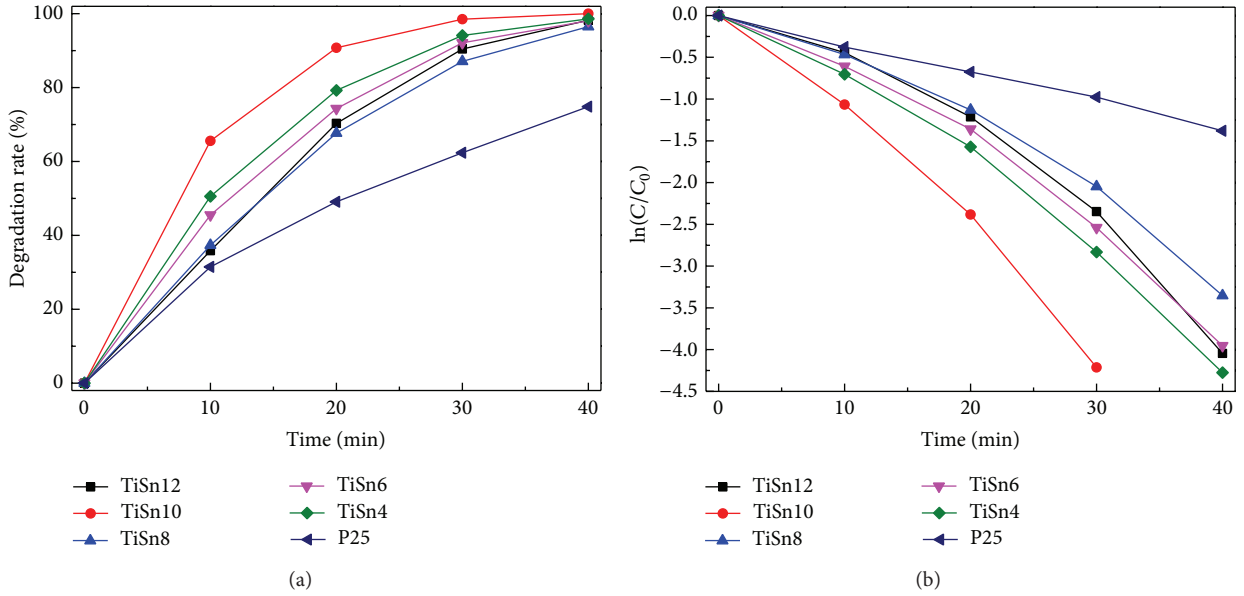

Figure 5: The photocatalytic degradation rate (a) and the pseudo-first-order kinetics (b) of the prepared samples and Degussa P25.

Table 1: The textural properties of the investigated catalysts.

Samples	Calcination temperature (°C)	Surface area[a] (m^2/g)	V_{tot} (cm^3/g)	$D_{BJH\text{-}ads}$[b] (nm)
TiSn12	80	96	0.22	7.7
TiSn10	80	73	0.23	10.9
TiSn8	80	162	0.51	10.7
TiSn6	80	106	0.32	10.3
TiSn4	80	71	0.28	13.9

[a]Multipoint BET surface area.
[b]Maximum of BJH pore diameter as determined from the adsorption branch.

Table 2: Absorption (in dark) and photodegradation rate (under UV light) of RB dye by different catalysts within 30 min.

Samples	TiSn12	TiSn10	TiSn8	TiSn6	TiSn4
Absorption (%)	47.0	60.4	51.4	51.9	54.5
Degradation rate (%)	90.4	98.5	87.1	92.1	94.1

doping and hierarchical macroporous-mesoporous structure. And, for these prepared samples, the relative order of photodegradation rate of RB dye solutions is TiSn10 > TiSn4 > TiSn6 ≈ TiSn12 > TiSn8. Although the samples TiSn6 and TiSn8 possess high surface area and pore volume (Table 1), they exhibit lower degradation effect. The lower activity of these two samples may be related to the smaller average pore size, which leads to the less absorption of RB dye compared with the samples TiSn10 and TiSn4 (Table 2). Furthermore, the photocatalytic activity of the sample TiSn10 is obviously higher than that of TiSn4. This may be owing to the lack of anatase phase in TiSn4, which is photocatalytic active phase that considered a predominant factor in influencing the photodegradation process. However, the sample TiSn4 with predominant rutile phase exhibits higher degradation rate than the sample TiSn6 with main anatase phase. This is possibly due to the increase of SnO_2 content in TiSn4, which leads to more Sn doping, forming smaller energy gap among the band gap of TiO_2, producing more electron-hole pairs, and thus improving the photocatalytic activity [13]. Figure 5(b) depicts the approximate linear relationship of $\ln(C/C_0)$ versus irradiation time t for the different samples, which indicates the photodegradation process of RB dye can be considered as a pseudo-first-order kinetics reaction. And the apparent rate constants were calculated to be 0.03385, 0.10032, 0.09149, 0.0764, 0.13363, and 0.09023 min^{-1} for pure TiO_2 (P25), TiSn4, TiSn6, TiSn8, TiSn10, and TiSn12 photocatalysts, respectively.

Figure 6 shows the absorption spectra of RB dye solution over the sample TiSn10. From Figure 6, it can be seen that the RB dye solution exhibits an obvious absorption peak at 553 nm at zero time, and the absorbance of RB dye solution at 553 nm is basically reduced to zero within 30 min, indicating the effective photodegradation of RB dye under the catalysis of TiSn10. On the other hand, the absorption peak gradually shifts to left with prolonged irradiation time, then stays around at λ = 496 nm (the absorption peak of one intermediate) at 40 min, and finally disappears within 70 min. This demonstrates that the RB dye in solution is degraded completely within 30 min, and the whole RB dye along with its intermediate products is fully degraded within 70 min.

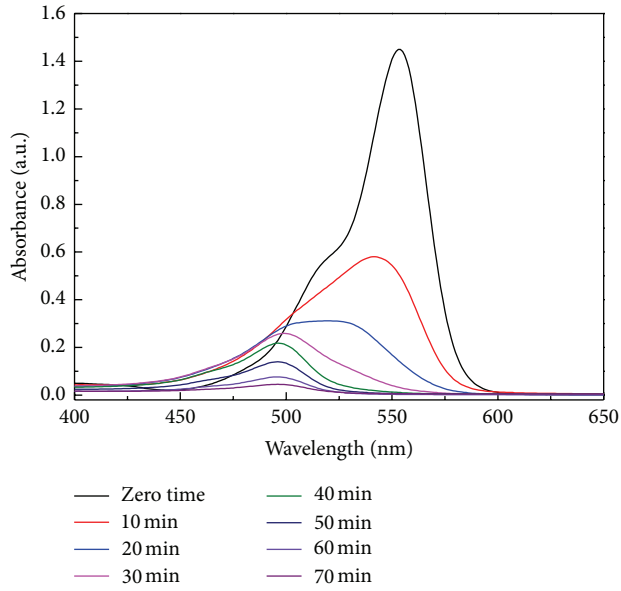

Figure 6: The absorption spectra of Rhodamine B solution over TiSn10.

4. Conclusions

The photocatalytic degradation of Rhodamine B dye was successfully carried out under UV irradiation over porous TiO_2-SnO_2 nanocomposites prepared by hydrothermal method by using polystyrene microspheres as template. The photocatalytic activities exhibit an order of TiSn10 > TiSn4 > TiSn6 ≈ TiSn12 > TiSn8 > pure TiO_2 (P25). The observed high photocatalytic activity is comprehensively affected by the molar ratios of Ti/Sn, hierarchical macroporous-mesoporous structure, and high surface area.

Conflict of Interests

The authors have no conflict of interests in relation to the instrumental companies mentioned in this paper directly or indirectly.

Acknowledgments

This work was supported by the National Natural Science Foundation of China (51172065) and State Key Laboratory Cultivation Base for Gas Geology and Gas Control (WS2013B03).

References

[1] S. Eftekhari, A. Habibi-Yangjeh, and S. H. Sohrabnezhad, "Application of AlMCM-41 for competitive adsorption of methylene blue and rhodamine B: thermodynamic and kinetic studies," *Journal of Hazardous Materials*, vol. 178, no. 1–3, pp. 349–355, 2010.

[2] X. Xue, X. He, and Y. Zhao, "Adsorptive properties of acid-heat activated rectorite for Rhodamine B removal: equilibrium, kinetic studies," *Desalination and Water Treatment*, vol. 37, no. 1–3, pp. 259–267, 2012.

[3] A. R. Tehrani-Bagha, N. M. Mahmoodi, and F. M. Menger, "Degradation of a persistent organic dye from colored textile wastewater by ozonation," *Desalination*, vol. 260, no. 1–3, pp. 34–38, 2010.

[4] R. G. Saratale, G. D. Saratale, J. S. Chang, and S. P. Govindwar, "Decolorization and biodegradation of reactive dyes and dye wastewater by a developed bacterial consortium," *Biodegradation*, vol. 21, no. 6, pp. 999–1015, 2010.

[5] M. H. Rasoulifard, S. M. M. Doust Mohammadi, A. Heidari, and G. H. Shahverdizadeh, "Photocatalytic degradation of acid red 14 from contaminated water using immobilized TiO_2 nanoparticles on glass beads activated by UV/peroxydisulfate," *Desalination and Water Treatment*.

[6] B. Esen, T. Yumak, A. Sinağ, and T. Yildiz, "Investigation of photocatalytic effect of SnO_2 nanoparticles synthesized by hydrothermal method on the decolorization of two organic dyes," *Photochemistry and Photobiology*, vol. 87, no. 2, pp. 267–274, 2011.

[7] J. C. Colmenares and R. Luque, "Heterogeneous photocatalytic nanomaterials: prospects and challenges in selective transformations of biomass-derived compounds," *Chemical Society Reviews*, vol. 43, no. 3, pp. 765–778, 2014.

[8] X. Chen and S. S. Mao, "Titanium dioxide nanomaterials: synthesis, properties, modifications and applications," *Chemical Reviews*, vol. 107, no. 7, pp. 2891–2959, 2007.

[9] Z. Liu, Y. Wang, W. Chu, Z. Li, and C. Ge, "Characteristics of doped TiO_2 photocatalysts for the degradation of methylene blue waste water under visible light," *Journal of Alloys and Compounds*, vol. 501, no. 1, pp. 54–59, 2010.

[10] F. E. Oropeza, B. Davies, R. G. Palgrave, and R. G. Egdell, "Electronic basis of visible region activity in high area Sn-doped rutile TiO_2 photocatalysts," *Physical Chemistry Chemical Physics*, vol. 13, no. 17, pp. 7882–7891, 2011.

[11] X. Zhang, G. Zhou, H. Zhang, C. Wu, and H. Song, "Characterization and activity of visible light-driven TiO_2 photocatalysts co-doped with nitrogen and lanthanum," *Transition Metal Chemistry*, vol. 36, no. 2, pp. 217–222, 2011.

[12] M. Habib, M. Shahadat, N. Bahadur, I. Ismail, and A. Mahmood, "Synthesis and characterization of ZnO-TiO_2 nanocomposites and their application as photocatalysts," *International Nano Letters*, vol. 3, no. 1, pp. 1–8, 2013.

[13] A. I. Martínez, D. R. Acosta, and G. Cedillo, "Effect of SnO_2 on the photocatalytical properties of TiO_2 films," *Thin Solid Films*, vol. 490, no. 2, pp. 118–123, 2005.

[14] J. Liqiang, F. Honggang, W. Baiqi et al., "Effects of Sn dopant on the photoinduced charge property and photocatalytic activity of TiO_2 nanoparticles," *Applied Catalysis B*, vol. 62, no. 3-4, pp. 282–291, 2006.

[15] C. Xiong and K. J. Balkus Jr., "Mesoporous molecular sieve derived TiO_2 nanofibers doped with SnO_2," *Journal of Physical Chemistry C*, vol. 111, no. 28, pp. 10359–10367, 2007.

[16] M. F. Abdel-Messih, M. A. Ahmed, and A. S. El-Sayed, "Photocatalytic decolorization of Rhodamine B dye using novel mesoporous SnO_2-TiO_2 nano mixed oxides prepared by sol-gel method," *Journal of Photochemistry and Photobiology A*, vol. 260, pp. 1–8, 2013.

[17] J. Du, G. Zhao, H. Pang, Y. Qian, H. Liu, and D. J. Kang, "A template method for synthesis of porous Sn-doped TiO_2 monolith and its enhanced photocatalytic activity," *Materials Letters*, vol. 93, pp. 419–422, 2013.

[18] X.-D. Wang, P. Dong, and G.-Y. Yi, "Evaporation self-assembly method to fabricate high-quality polystyrene microsphere colloid crystal," *Acta Physica Sinica*, vol. 55, no. 4, pp. 2092–2098, 2006.

[19] X.-D. Wang, G.-Y. Yi, and Y. Liu, "Preparation of Al_2O_3 catalytic material with run-through-macropore network structure," *Chemical Journal of Chinese Universities*, vol. 30, no. 2, pp. 349–354, 2009.